Journal of Applied Physics

RESEARCH ARTICLE | MAY 15 2023

Twofold increase in the sensitivity of Er^{3+}/Yb^{3+} Boltzmann thermometer

Aleksandar Ćirić ; Thomas van Swieten ; Jovana Periša ; Andries Meijerink ; Miroslav D. Dramićanin

J. Appl. Phys. 133, 194501 (2023)
https://doi.org/10.1063/5.0149757

Journal of Applied Physics METHOD scitation.org/journal/jap

Twofold increase in the sensitivity of Er^{3+}/Yb^{3+} Boltzmann thermometer

Cite as: J. Appl. Phys. 133, 194501 (2023); doi: 10.1063/5.0149757
Submitted: 8 March 2023 · Accepted: 17 April 2023 ·
Published Online: 15 May 2023

View Online Export Citation CrossMark

Aleksandar Ćirić,[1,a)] Thomas van Swieten,[2] Jovana Periša,[1] Andries Meijerink,[2] and Miroslav D. Dramićanin[1]

AFFILIATIONS

[1]Centre of Excellence for Photoconversion, Vinča Institute of Nuclear Sciences—National Institute of the Republic of Serbia, University of Belgrade, P.O. Box 522, Belgrade 11001, Serbia
[2]Debye Institute For Nanomaterials Science, Utrecht University, Princetonplein 1, 3584 CC, The Netherlands

[a)]**Author to whom correspondence should be addressed:** aleksandar.ciric@ff.bg.ac.rs

ABSTRACT

Luminescence thermometry is the most versatile remote temperature sensing technique and can be employed from living cells to large surfaces and from cryogenic temperatures to the melting points of metals. Ongoing research aims to optimize the sensitivity of the ratio between the emission intensity from two coupled excited states. However, this approach is inherently limited to temperature-dependent processes involving only the excited states. Here, we develop a novel measurement technique, called luminescence intensity ratio squared (LIR^2) for the Yb^{3+}/Er^{3+} pair, that combines the temperature sensitivity of ground- and excited-state populations. We use $Y_3Al_5O_{12}:Er^{3+},Yb^{3+}$ nanoparticles as a promising model system with both visible and infrared emissions. To apply our method, we record two luminescence spectra at different excitation wavelengths and determine the LIR^2 using one emission in each of the two spectra. The LIR^2 testing with $Y_3Al_5O_{12}$ nanoparticles showed a sensitivity increase of 70% in the visible region and an impressive 230% increase in the NIR region compared to the conventional LIR method. This enhances the measurement precision by a factor of 1.5–2.5. The LIR^2 based on the visible upconversion emission is particularly useful for measurements of high temperatures, while the LIR^2 based on the downshifted ~1.5 μm emission may revolutionize temperature measurements of biological samples in the range of physiological temperatures.

I. INTRODUCTION

The luminescence intensity ratio (LIR) is the most common metric in luminescence thermometry. It typically uses the ratio between emission intensities from two thermally coupled states as a measure of the local temperature.[1,2] The advantages of LIR over other luminescence thermometry methods are numerous. For example, it is highly sensitive and self-referenced.[3] It is unaffected by instabilities in the excitation source and the detection device.[4] The implementation only requires relatively cheap optical and electronic components and it can be easily used in industrial applications.[5–7]

Among the different types of materials used for LIR thermometry, phosphors activated by trivalent lanthanides (Ln^{3+}) have proven to be particularly well suited due to their high number of closely lying excited states that show emission from the ultraviolet (UV) to the near-infrared (NIR).[8,9] Their narrow emission bands at well-defined wavelengths lead to small spectral overlaps and allow for the accurate determination of LIRs. The syntheses of these materials are well-mastered, and they can be prepared in different forms, from bulk single crystals to nanoparticles.[10] For these reasons, Ln^{3+} phosphors are, by far, the most exploited materials in luminescence thermometry.

Among all Ln^{3+} phosphors, Er^{3+} is one of the most popular ions in LIR thermometry.[11] With this ion, thermometry can be realized in three distinctive spectral regions and has already found valuable applications across many fields, from engineering to biomedicine.[12] Transitions from the $^2H_{11/2}$ and $^4S_{3/2}$ excited states to the $^4I_{15/2}$ ground state provide green emissions, which strongly depend on temperature.[13] Transitions from the same excited states to the $^4I_{13/2}$ state lead to emissions in the near-infrared at around 800 nm.[14,15] These NIR emissions, however, have low intensities and are often barely measurable. The LIR based on the strong emissions from Stark components of the $^4I_{13/2}$ state to the $^4I_{15/2}$ ground state operates at around 1540 nm, in the important third biological

transparency window (BW-III).[16–18] Due to the non-linear spectral distortions, when measured within a tissue, the emissions used for LIR must be spectrally close so that the differences between the ratio of intensities are weakly affected.[19]

The main weakness of Ln^{3+}-based LIR thermometers is a sensitivity limit imposed by the energy difference between thermally coupled emissive states, which causes relatively large temperature measurement uncertainties. The relative sensitivity is around 1.2% K^{-1} for Er^{3+} LIRs in the green and NIR spectral regions, and 0.3% K^{-1} for the BW-III LIR. To overcome the limitations in sensitivity, two approaches have recently been introduced. The first is based on emissions from the energetically higher Ln^{3+} excited levels[14,20–23] and provides a gain in sensitivity due to a larger energy difference between the emissive states. However, the intensities of these emissions are weak, which results in higher measurement uncertainties. In addition, they work only at high temperatures, which are required for thermal equilibrium between the observed excited states. For example, for the Eu^{3+} $^5D_1$–$^5D_0$ levels, the calculated relative sensitivity is 2.8% K^{-1} at 300 K, but the large energy gap prevents Boltzmann equilibrium at 300 K.[24–26] When equilibrium is established at higher temperatures, the very low emission intensities from the higher $^5D_1$ level introduce large uncertainties in the measured intensity. In the second approach introduced by Malta *et al.*,[27] named the dual-excited single-band ratiometric (SBR) method,[28–30] luminescence is sequentially excited at two different wavelengths, which induces absorption from the ground state or a state slightly above it. Then, the LIR is determined from the ratio of intensities of one emission band excited from the ground and from the slightly higher excited state thermally coupled to it. Thus, thermal coupling between the absorbing states makes this LIR sensitive to temperature. This provides a new range of thermally coupled states to choose from in the design of thermometers, but the gain in sensitivity is modest since the energy differences are similar to those exploited in the conventional LIR.[31]

Our group recently introduced the luminescence intensity squared (LIR^2) method, which combines the conventional LIR and SBR methodologies to increase the relative sensitivity while maintaining the intensity uncertainties of LIR- and SBR-based measurements and thermal equilibrium in a relatively low-temperature range.[32] Again, a measurement requires the acquisition of two luminescence spectra at different excitation wavelengths, but, in this case, the LIR is determined from only one emission band in each spectrum instead of the total spectrum. Specifically, we are interested in the emission intensity of the higher emitting state after excitation from the higher absorbing state and in the emission intensity of the lower-emitting state after excitation from the lower-absorbing state. At elevated temperatures, the ratio between these emissions increases due to thermal coupling between both the absorbing and the emitting state, which drastically increases the sensitivity compared to the individual ratios. The new technique gives high relative sensitivities similar to that for a ΔE that is the sum of the two energy differences involved but now allows for Boltzmann equilibrium, a temperature range where this is not possible for the high ΔE values and with high emission intensities resulting from the relatively high populations of the higher excited states determined by the two energy differences.

Herein, we engineered a LIR^2 luminescent thermometer with the Er^{3+}/Yb^{3+} luminescent pair with improved performance in both the visible and NIR spectral range. For this purpose, we used a well-known $Y_3Al_5O_{12}$: Er^{3+}/Yb^{3+} phosphor material. Yb^{3+} is especially famed for its sensitization of different Ln^{3+} ions, providing them with sufficient light absorption for intense emission. In the LIR^2, this ion takes on an additional and vital function by affording excitations from the two thermalized Stark components of its $^2F_{7/2}$ ground state. We measured emission and analyzed LIR, SBR, and LIR^2 thermometer performances with the same material and showed LIR^2 superiority over the two other approaches in terms of sensitivity, temperature resolution, and measurement range.

II. EXPERIMENTAL

$Y_3Al_5O_{12}$ nanoparticles doped with 10% Yb and 2% Er (with respect to Y) were synthesized via the modified Pechini method described in detail in Ref. 16. The material crystal structure and phase purity are checked by x-ray diffraction measurements (Rigaku SmartLab instrument; Cu-$Ka_{1,2}$ radiation, 0.1540 nm) (Fig. S1 in the supplementary material). It is formed from particles of around 35 nm in diameter according to transmission electron microscopy (Fig. S1 in the supplementary material), performed on TESCAN MIRA3 and Philips CM-20 SuperTwin, respectively (the material was coated with Au by a typical sputtering process using Polaron SC502—Fison Instruments).

The sample was excited with a focused Ekspla NT342B OPO laser. The laser gives short (~10 ns) pulses with typical pulse energies of 10 mJ at wavelengths that can be tuned from 210 to 2200 nm. For the excitation spectra, the relevant emission lines of Er^{3+} were selected using a Triax 550 monochromator and recorded with an R928 photomultiplier tube [see Fig. S2(b) in the supplementary material]. The visible and infrared Er^{3+} luminescence was recorded using a fiber-coupled Andor Kymera 193i spectrometer, equipped with an air-cooled Andor iVac Front-illuminated deep depletion CCD and a water-cooled Andor iDus 1.7 μm InGaAs CCD, respectively. The heating and cooling of the samples were achieved with a Linkam THMS600 microscope stage equipped with a liquid nitrogen pump.

The diffuse-reflectance of YAG:Er^{3+}/Yb^{3+} was recorded by Shimadzu UV-2600 [see Fig. S1(a) in the supplementary material]. The absorption of Yb^{3+} at different temperatures was estimated by the Kubelka–Munk function, F(R), from the measurement of diffuse reflection, R, using an integrating sphere and an Ocean Insight FX spectrometer,[5,33]

$$F(R) = \frac{(1-R)^2}{2R}. \tag{1}$$

III. THEORY

The conventional LIR is constructed as the ratio of intensities of emissions from energetically higher (H) and energetically lower (L) excited states. If emitting levels are in thermal equilibrium, meaning that the thermal energy can effectively populate H from the L state faster than radiative decay from either state, then LIR follows the Boltzmann distribution given by[1]

$$LIR(T) = \frac{I_H(T)}{I_L(T)} = B\exp\left(-\frac{\Delta E}{kT}\right), \tag{2}$$

where B is the temperature invariant parameter that depends on the properties of a host material and an activator ion,[25] ΔE represents the energy difference between the thermalized levels from which emissions occur, and $k = 0.695\ \mathrm{cm^{-1}\ K^{-1}}$ is the Boltzmann constant.

The SBR is constructed as the ratio of emission intensities obtained under excitations from energetically higher and lower states (these excitation processes are often termed ground-state absorption and excited-state absorption, respectively). The mathematical formulation is the same as in a conventional LIR [Eq. (2)]. The only difference is that in this case, ΔE represents the energy difference between the two thermally coupled levels from which the excitation occurs.

The luminescence intensity ratio squared ($\mathrm{LIR^2}$) is a recently introduced luminescence thermometry method that combines LIR and SBR approaches.[32] It is described by Eq. (2), where ΔE is the sum of energy differences between the thermalized emission and thermalized excitation states.

The relative sensitivity of LIR and SBR Boltzmann thermometers defined by Eq. (2) has a simple form of[34]

$$S_r(T) = \frac{1}{LIR}\left|\frac{\partial LIR}{\partial T}\right| \times 100\% = \frac{\Delta E}{kT^2} \times 100\%. \tag{3}$$

The temperature resolution (uncertainty in temperature) is given by[35]

$$\Delta T(T) = \frac{\sigma_r(T)}{S_r(T)}, \tag{4}$$

where σ_r is the relative uncertainty in a measurement, obtained as a relative standard deviation in a series of measurements.

The uncertainties of measurement for LIR can be estimated from uncertainties in the emission intensity measurements of transitions involved in the calculation,[36,37]

$$\sigma_r(LIR) = \sqrt{\sigma_r^2(I_H) + \sigma_r^2(I_L)}\,. \tag{5}$$

IV. RESULTS AND DISCUSSION

A. Engineering of $\mathrm{Er^{3+}/Yb^{3+}}$ $\mathrm{LIR^2}$ thermometers for visible and near-infrared spectral regions

To experimentally verify the superior sensitivity of the $\mathrm{LIR^2}$ method that was introduced by some of us in Ref. 32, we chose YAG: $\mathrm{Er^{3+}/Yb^{3+}}$ as the model system. The diffuse reflection spectra of YAG: $\mathrm{Er^{3+}/Yb^{3+}}$ recorded at various temperatures are presented in Fig. S2 in the supplementary material, revealing peaks that correspond to the absorptions from the $^2F_{7/2}$ ground level of $\mathrm{Yb^{3+}}$ to its only excited 4f level $^2F_{5/2}$. The crystal field splitting causes sublevels (known as Stark levels) which are marked with numbers from 1 to 7, where sublevels 1 to 4 form $^2F_{7/2}$ and sublevels 5 to 7 form $^2F_{5/2}$. At elevated temperatures, we observe an increase in the $3 \rightarrow 5$ excitation intensity at 1031 nm and a decrease in the $1 \rightarrow 7$ excitation intensity at 916 nm [see Fig. 1(a)]. This temperature-dependent behavior is caused by thermal coupling between the sublevels of $^2F_{7/2}$ following Boltzmann statistics. We choose the $1 \rightarrow 7$ and $3 \rightarrow 5$ transitions for the excitation part of $\mathrm{LIR^2}$ (and SBR) on YAG:$\mathrm{Er^{3+}/Yb^{3+}}$ [see Fig. 1(b)], not only due to their opposite trends with temperature, but also because those transitions do not overlap with other transitions between the various sublevels of $\mathrm{Yb^{3+}}$.

In the visible region, the emission spectra at various temperatures upon 916 nm excitation present the typical $\mathrm{Er^{3+}}$ upconversion emission from $^2H_{11/2}$ and $^4S_{3/2}$, enabled by energy transfer from $^2F_{5/2}$ of $\mathrm{Yb^{3+}}$ to $\mathrm{Er^{3+}}$ [Fig. 1(c)].[38–40] We observe a strong increase of the relative $^2H_{11/2}$ intensity with temperature, which we again explain by thermal coupling, this time between $^2H_{11/2}$ and $^4S_{3/2}$. We use the integrated intensity of these emissions for the conventional LIR ($\mathrm{LIR_a}$), as presented in Fig. 1(d) (left). The energy gap between the emissions in $\mathrm{LIR_a}$ corresponds to the energy difference between the $^2H_{11/2}$ and $^4S_{3/2}$ levels, and it is approximately equal to 700 $\mathrm{cm^{-1}}$, regardless of the host matrix.[11,41] The emission spectra of $\mathrm{Er^{3+}}$ under excitation at 1031 nm are presented in Fig. S3(a) in the supplementary material. The emission from $^4S_{3/2}$ recorded at this different excitation wavelength can be used for the SBR ($\mathrm{LIR_b}$) method: the $^4S_{3/2} \rightarrow {}^4I_{15/2}$ emission is observed upon excitation at 916 and 1031 nm and their ratio is taken for $\mathrm{LIR_b}$. Note that, we assume here that the upconversion intensity is proportional to the $\mathrm{Yb^{3+}}$ excited state population which is not trivial for an upconversion process and only holds in an excitation density limit. The energy gap corresponds to the energy difference between the sublevels 1 and 3 of $\mathrm{Yb^{3+}}$ [see Fig. 1(d) (middle)]. Note that, unlike the energy difference between the 4f spin–orbit levels, the position of the crystal field sublevels greatly depends on the host matrix and allows for additional flexibility in finding suitable lanthanide–host combinations for $\mathrm{LIR^2}$ thermometry optimized for specific temperature ranges. According to the literature, the energy difference between sublevels 1 and 3 in YAG is 612 $\mathrm{cm^{-1}}$.[42]

In the NIR region, we observe a single (downshifting) emission from the first excited level of $\mathrm{Er^{3+}}$, $^4I_{13/2}$, to the ground level, $^4I_{15/2}$, centered at ca. 1.5 μm [see Fig. 1(e)].[43,44] The conglomerate emission $^4I_{13/2} \rightarrow {}^4I_{15/2}$ is composed of multiple, overlapping components, that can be classified into two groups. Peaks between 1450 and 1500 nm and beyond 1555 nm increase with temperature as they originate from the energetically higher Stark sublevels of the $^4I_{13/2}$ level (H), and peaks between 1500 and 1555 nm decrease in intensity as they originate from the lower Stark sublevels (L).[16] We determine $\mathrm{LIR_a}$ from the H and L emission upon excitation at 916 nm. For $\mathrm{LIR_b}$, we use the $^4I_{13/2} \rightarrow {}^4I_{15/2}$ emission recorded upon excitations at 916 and 1031 nm, analogous to the $\mathrm{LIR_b}$ method in the visible region [see Fig. 1(f)]. For $\mathrm{LIR^2}$, first, the material is excited by the $3 \rightarrow 5$ pathway in $\mathrm{Yb^{3+}}$, and the observable is the intensity from the H sublevels of $\mathrm{Er^{3+}}$. In the second step, the $1 \rightarrow 7$ excitation is performed, while observing the L intensity. Analogous to the method for $\mathrm{Er^{3+}/Yb^{3+}}$ in the visible region, the ratio of intensities obtained in those two steps is used for the $\mathrm{LIR^2}$ method, and the effective energy gap is equal to the sum of separate energy gaps: between the H and L sublevels of $\mathrm{Er^{3+}}$, and 1 and 3 sublevels of $\mathrm{Yb^{3+}}$ (see below for further explanation).

B. Performance comparison of LIR, SBR, and $\mathrm{LIR^2}$ $\mathrm{Er^{3+}/Yb^{3+}}$ $\mathrm{LIR^2}$ thermometers

Emission spectra were recorded for YAG: $\mathrm{Er^{3+}/Yb^{3+}}$ under both 916 and 1031 nm excitations in the visible and NIR in the

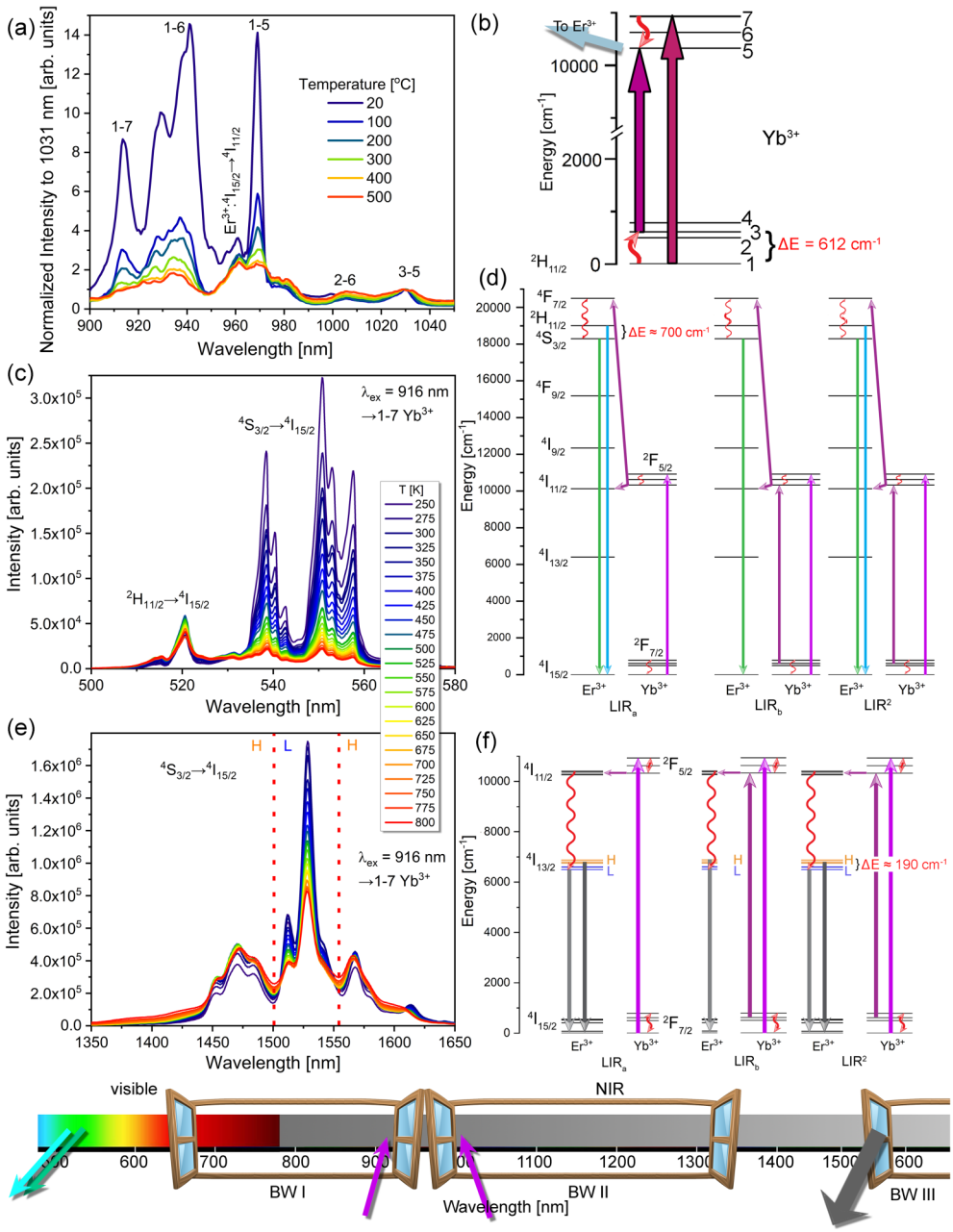

FIG. 1. (a) Temperature-dependent excitation spectrum of Yb^{3+} and (b) the corresponding energy diagram.[45] (c) Temperature-dependent emission spectra in (c) visible and (e) NIR, under 916 nm excitation. Energy level diagram of LIR_a, LIR_b, and LIR^2 methods for Yb^{3+}/Er^{3+} in the (d) visible range by upconversion and (f) the NIR range by downshifting. Upward-wavy arrows represent excitations by thermal energy, downward-wavy arrows are non-radiative de-excitations, upward-straight arrows are excitations by photons, and downward-straight arrows are the emission of photons. The horizontal arrows from Yb^{3+} to Er^{3+} represent energy transfer.

300–800 K temperature range. In addition, at three temperatures (310, 650, and 800 K), a large number of spectra was recorded to determine the uncertainties in the measured intensities. From the spectra given in Fig. 1(b) and Fig. S3(a) in the supplementary material in the visible, and Fig. 1(e) and Fig. S3(b) in the supplementary material in the NIR region, all three methods LIR_a, LIR_b, and LIR^2 [by mechanisms presented in Figs. 1(d) and 1(f)], were employed to estimate the performance of each method in both

spectral regions for temperature sensing. Each method is fitted by the Boltzmann relation in Eq. (2).

The LIR_a, LIR_b, and LIR^2, in the visible region of YAG:Er^{3+}/Yb^{3+}, are then given by, respectively,

$$LIR_a^{\mathrm{vis}} = \frac{I(^2H_{11/2} \rightarrow {}^4I_{15/2}, \lambda_{ex} = 916\ \mathrm{nm})}{I(^4S_{3/2} \rightarrow {}^4I_{15/2}, \lambda_{ex} = 916\ \mathrm{nm})} = B_a^{\mathrm{vis}} \exp\left(-\frac{\Delta E_a^{\mathrm{vis}}}{kT}\right), \tag{6}$$

$$LIR_b^{\mathrm{vis}} = \frac{I(^4S_{3/2} \rightarrow {}^4I_{15/2}, \lambda_{ex} = 1031\ \mathrm{nm})}{I(^4S_{3/2} \rightarrow {}^4I_{15/2}, \lambda_{ex} = 916\ \mathrm{nm})} = B_b^{\mathrm{vis}} \exp\left(-\frac{\Delta E_b^{\mathrm{vis}}}{kT}\right), \tag{7}$$

$$LIR^{2,\mathrm{vis}} = \frac{I(^2H_{11/2} \rightarrow {}^4I_{15/2}, \lambda_{ex} = 1031\ \mathrm{nm})}{I(^4S_{3/2} \rightarrow {}^4I_{15/2}, \lambda_{ex} = 916\ \mathrm{nm})} = B_{ab}^{\mathrm{vis}} \exp\left(-\frac{\Delta E_{ab}^{\mathrm{vis}}}{kT}\right). \tag{8}$$

Equations (6)–(8) were fitted to the experimental data and the results are given in Figs. 2(a)–2(c), respectively. In the NIR region, analogous equations are used,

$$LIR_a^{\mathrm{NIR}} = \frac{I(^4\mathrm{I}_{13/2}(\mathrm{H}) \rightarrow {}^4\mathrm{I}_{15/2}, \lambda_{\mathrm{ex}} = 916\ \mathrm{nm})}{I(^4I_{13/2}(L) \rightarrow {}^4I_{15/2}, \lambda_{ex} = 916\ \mathrm{nm})} = B_a^{\mathrm{NIR}} \exp\left(-\frac{\Delta E_a^{\mathrm{NIR}}}{kT}\right), \tag{9}$$

$$LIR_b^{\mathrm{NIR}} = \frac{I(^4I_{13/2} \rightarrow {}^4I_{15/2}, \lambda_{ex} = 1031\ \mathrm{nm})}{I(^4I_{13/2} \rightarrow {}^4I_{15/2}, \lambda_{ex} = 916\ \mathrm{nm})} = B_b^{\mathrm{NIR}} \exp\left(-\frac{\Delta E_b^{\mathrm{NIR}}}{kT}\right), \tag{10}$$

$$LIR^{2,\mathrm{NIR}} = \frac{I(^4I_{13/2}(H) \rightarrow {}^4I_{15/2}, \lambda_{ex} = 1031\ \mathrm{nm})}{I(^4I_{13/2}(L) \rightarrow {}^4I_{15/2}, \lambda_{ex} = 916\ \mathrm{nm})} = B_{ab}^{\mathrm{NIR}} \exp\left(-\frac{\Delta E_{ab}^{\mathrm{NIR}}}{kT}\right), \tag{11}$$

and the experimental data are fitted in Figs. 2(d)–2(f). As it was predicted, the sum of the energy gaps of the LIR_a and LIR_b methods is approximately equal to the effective energy gap of LIR^2, both in the visible and NIR regions.

A comparison of the relative sensitivities of LIR^2 with the LIR_a and LIR_b methods is shown in Fig. 3. The relative sensitivities were obtained from Eq. (3) by using the ΔE values fitted in Fig. 2. The relative sensitivity of the LIR^2 method in both visible and NIR is equal to the sum of the relative sensitivities of LIR_a and LIR_b. According to Eq. (3), this was anticipated, as the effective energy gaps obtained from the fitting in Figs. 2(c) and 2(f) are equal to the sums of energy gaps of LIR_a and LIR_b. This presents a significant increase. In the visible region, the sensitivity is increased by ~70%, and the LIR^2 method could show the largest perspective at higher temperatures, where the LIR_a and LIR_b methods demonstrate low sensitivities (e.g., 0.14% K^{-1} of LIR_a vs 0.24% K^{-1} of LIR^2). In the NIR, with potential temperature sensing applications on the biological samples with nanoparticles, the LIR_a method suffers from a minuscule energy gap of ~180 cm^{-1}, and thus, the low relative sensitivity. At the normal body temperature of 310 K, this sensitivity is equal to 0.27% K^{-1}. Here, LIR_b is more promising, as at the same temperature, it provides 0.36% K^{-1}. LIR^2 is again the best method, as at 310 K, the relative sensitivity is 0.61% K^{-1}, which is a ~230% increase over the sensitivity of the conventional LIR method. Thus, LIR^2 shows a strong potential to be used as a NIR–NIR nanothermometer in the physiological range. One should note, however, that the fitted value of the energy difference between levels in the LIR_b method for the NIR [Fig. 2(e)] is smaller than for the visible spectral range [Fig. 2(b)]. At the moment, it is not clear what the explanation for this is. It may be related to some overlap of the H and L emission lines and the choice of the integration areas for the H and L spectral regions. In any case, this does not affect the applicability of the method. Interestingly, even with this discrepancy, the energy differences obtained with the LIR^2 method are the sums of the energy differences obtained with the LIR_a and LIR_b methods, in both NIR and visible thermometry measurements.

Relative uncertainties of the emission intensity measurements are determined at two temperatures (in the visible spectral region at higher temperatures of 650 K and 800 K; in the NIR region at a body temperature of 310 K, and at 650 K), Fig. S4 in the supplementary material. The obtained uncertainty values are approximately the same for all three methods in each spectral region (see Table S1 in the supplementary material). As the uncertainties, and consequently, temperature resolutions, depend on the experimental setup, the temperature resolutions presented in Table I are normalized to the temperature resolution obtained for the conventional LIR [see Eq. (S1) in the supplementary material], allowing a direct comparison of the methods regardless of the measurement conditions.

Results in Table I are in favor of the LIR^2 method at all temperatures and both in NIR and the visible range. Regarding the comparison between LIR_a and LIR_b, the former is better in the visible, and the latter, in the NIR region.

YAG:Er^{3+}/Yb^{3+} was selected as the testing material for the LIR^2 method due to the known high intensity of the $3 \rightarrow 5$ excitation of Yb^{3+}, even at room temperature. In other host lattices, the LIR^2 and LIR_b methods are less advantageous, as the absorptions from the sublevels 3 and 4 of Yb^{3+} can be very weak. The preferred material for LIR^2 and LIR_b of the Er^{3+}/Yb^{3+} system is the one with the high intensity of the excited state absorption in Yb^{3+}. This is analogous to the previously reported beneficial effect of higher transition probabilities for emission from the thermally populated higher excited state,[23] which is also fulfilled here for LIR_a^{vis} where the $^2H_{11/2}$–$^4I_{15/2}$ transition is known to have a higher oscillator strength than the $^4S_{3/2}$–$^4I_{15/2}$ transition. In general, higher transition probabilities from thermally populated states (both in excitation and emission) result in higher accuracies of LIR thermometers.

There are certain limitations to the application of the LIR^2 method. Although the YAG host was chosen as a well-known matrix, another potential candidate, YF_3, which has a lower phonon energy, did not show prominent Yb^{3+} Stark sublevels that increase with temperature in the excitation spectrum. Further investigation is required for the evaluation of which type of hosts can be used for LIR^2 with Yb^{3+}/Er^{3+}. The advantage of LIR over many other methods lies in readout being unperturbed by the fluctuations in excitation. Generally, an excitation lamp's intensity

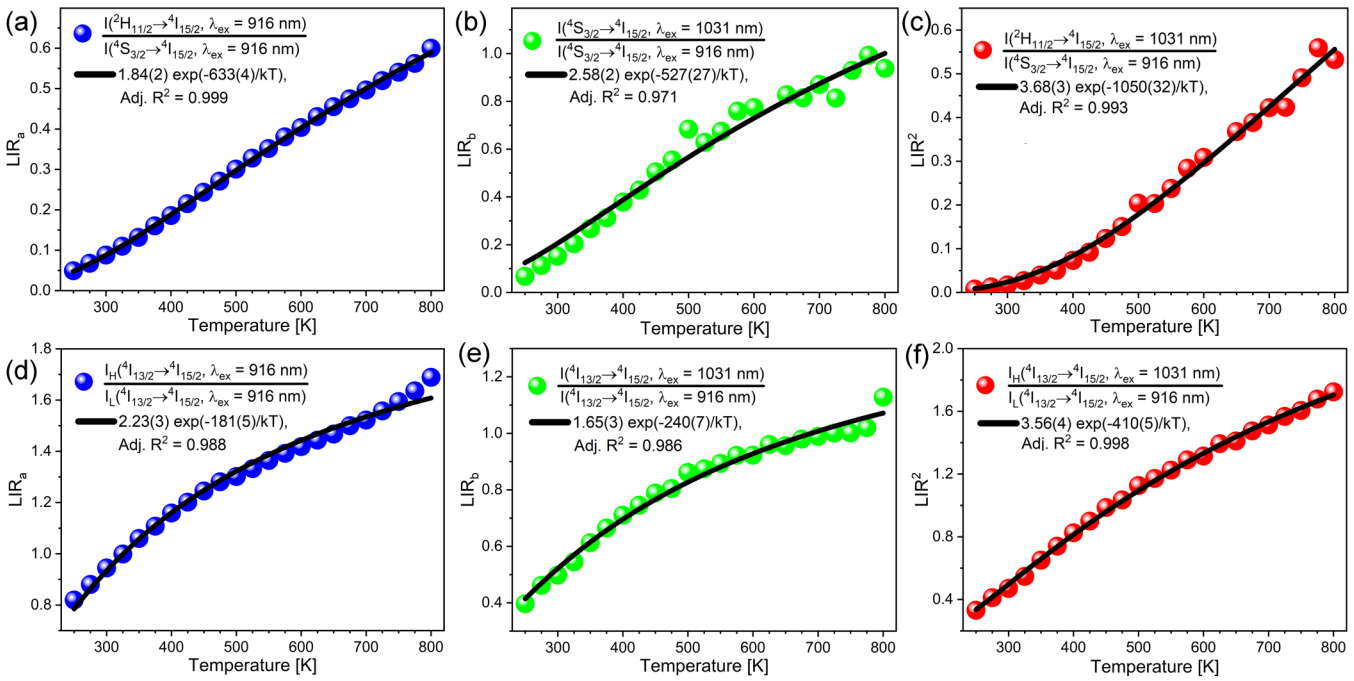

FIG. 2. (a) LIR_a, (b) LIR_b, (c) LIR^2 fit to the experimental data of the visible emissions, and (d) LIR_a, (e) LIR_b, and (f) LIR^2 of the NIR emissions of YAG:Yb^{3+}/Er^{3+}. Fits to the Boltzmann relation are obtained by the LumTHools software.[46]

fluctuates much more than that of a semiconductor laser. For LIR^2, it is recommended to use either high-stability lasers, semiconductor lasers that share the same power source, or simply perform measurements for a long-enough time so that random fluctuations in excitation average out. The speed and resolution at which reliable measurements can be performed is, however, mostly dependent on the experimental setup: excitation power and stability, optics, and detector system.[37] The difference in spectral responses when applied within a tissue in comparison to the LIR given in this paper is expected, but minimum, since the observed NIR emissions, are spectrally very close. Also, the water within the tissue has different (although slightly) absorption coefficients at excitations used for SBR.[47] Thus, it is expected that the 1031 nm excitation gets slightly weakened in comparison to the 916 nm if the probe is

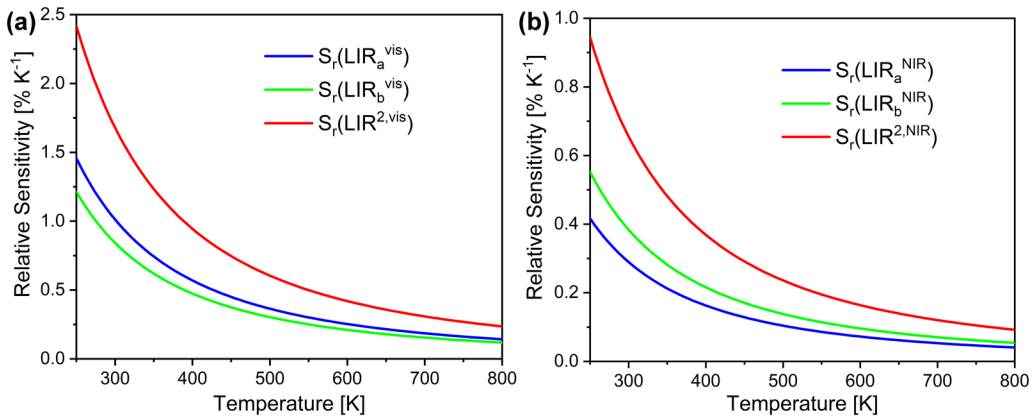

FIG. 3. Comparison of relative sensitivities for the LIR_a, LIR_b, and LIR^2 methods of YAG:Er^{3+}/Yb^{3+} in (a) visible, and (b) NIR regions.

TABLE I. Comparison of temperature resolutions in the NIR and visible regions, estimated at various temperatures, by the LIR_a, LIR_b, and LIR^2 methods, normalized to the temperature resolution of the conventional LIR_a method.

Region	NIR		Visible	
T (K)	310	650	650	800
S_r (LIR_a) (% K^{-1})	0.84	0.40	1.40	1.14
S_r (LIR_b) (% K^{-1})	1.11	0.53	1.17	0.95
S_r (LIR^2) (% K^{-1})	1.90	0.91	2.32	1.89
δT (LIR_a)	1.00	1.00	1.00	1.00
δT (LIR_b)	0.77	0.69	1.43	1.52
δT (LIR^2)	0.42	0.40	0.60	0.60

inserted too deep within the tissue. A slight excitation delay after each excitation sequence or using low-power lasers would prevent the self-heating of water within a tissue, yielding unreliable results. The obtained LIR within a tissue would be then equal to the LIR of the nanoparticles at an averaged depth within the tissue; however, further investigation on the topic and comparison with the well-established lifetime methods for biomedical applications[48] lies outside of the scope of this paper.

V. CONCLUSION

Conventional luminescence thermometry based on the LIR methods has limitations in sensitivity and precision imposed by the value of the energy gap between the thermalized levels. These limitations are mitigated in Er^{3+}/Yb^{3+} thermometers with a LIR^2 temperature read-out for both upconversion and downshifted emissions. The engineering of LIR^2 for the Er^{3+}/Yb^{3+} pair is based on the combination of the conventional LIR and SBR read-outs, which provides the simultaneous exploitation of thermalizations in both the ground and excited states, increasing the effective energy gaps while maintaining Boltzmann equilibrium and high emission intensities. As a result, a significant increase in sensitivity is obtained in both visible and NIR regions, while preserving low uncertainties in the emission intensity measurements, which ultimately results in a higher precision of the thermometer.

The drawback in comparison to the conventional LIR method is the necessity of using two excitation wavelengths. Thus, practical implementation requires a slightly more complex device than what is currently being used, but is aided by the availability of compact, cheap, and powerful diode lasers at almost any wavelength. The present demonstration of the feasibility of superior LIR^2 temperature sensing can be transferred to other Er^{3+}/Yb^{3+} doped hosts. Our future work will also include other well-known upconverting systems, such as Tm^{3+}/Yb^{3+} and Ho^{3+}/Yb^{3+}, while LIR^2 temperature sensing can also be extended to simple single ion downshifting schemes, such as Nd^{3+}. LIR^2 thermometry offers superior temperature precision and increased flexibility in both spectral and temperature ranges, which makes this new technique highly promising in the field of luminescence thermometry.

SUPPLEMENTARY MATERIAL

See the supplementary material for additional figures and equations that were mentioned in the manuscript, namely, SEM and XRD data, diffuse-reflectance spectra, temperature dependent spectra under 1031 nm excitation, uncertainties of measurement at each temperature, relative uncertainties, and an equation for the relative temperature resolution.

ACKNOWLEDGMENTS

This work was supported by the Ministry of Science, Technological Development and Innovation of the Republic of Serbia (No. 451-03-47/2023-01/200017). T.v.S. and A.M. gratefully acknowledge support by the Netherlands Center for Multiscale Catalytic Energy Conversion (MCEC), an NWO Gravitation Programme funded by the Ministry of Education, Culture and Science of the government of The Netherlands. The authors acknowledge Dr. Zoran Ristić for the diffuse reflection measurements.

AUTHOR DECLARATIONS

Conflict of Interest

The authors have no conflicts to disclose.

Author Contributions

Aleksandar Ćirić: Conceptualization (lead); Data curation (lead); Formal analysis (lead); Investigation (lead); Methodology (lead); Validation (lead); Visualization (lead); Writing – original draft (lead); Writing – review & editing (lead). **Thomas van Swieten:** Investigation (supporting); Writing – review & editing (supporting). **Jovana Periša:** Resources (lead). **Andries Meijerink:** Project administration (equal); Resources (equal); Supervision (equal); Writing – review & editing (equal). **Miroslav D. Dramićanin:** Conceptualization (supporting); Funding acquisition (equal); Project administration (equal); Supervision (equal); Writing – review & editing (equal).

DATA AVAILABILITY

The data that support the findings of this study are available from the corresponding author upon reasonable request.

REFERENCES

[1]S. A. Wade, S. F. Collins, and G. W. Baxter, "Fluorescence intensity ratio technique for optical fiber point temperature sensing," J. Appl. Phys. **94**, 4743 (2003).
[2]B. Bendel and M. Suta, "How to calibrate luminescent crossover thermometers: A note on 'quasi'-Boltzmann systems," J. Mater. Chem. C **10**, 13805 (2022).

[3]I. E. Kolesnikov, E. V. Afanaseva, M. A. Kurochkin, E. I. Vaishlia, E. Y. Kolesnikov, and E. Lähderanta, "Dual-center co-doped and mixed ratiometric $LuVO_4$:Nd^{3+}/Yb^{3+} nanothermometers," Nanotechnology **33**, 165504 (2022).
[4]X. Wang, O. S. Wolfbeis, and R. J. Meier, "Luminescent probes and sensors for temperature," Chem. Soc. Rev. **42**, 7834 (2013).
[5]K. T. V. Grattan and B. T. Meggitt, *Optical Fiber Sensor Technology* (Springer Netherlands, Dordrecht, 1999).
[6]S. W. Allison and G. T. Gillies, "Remote thermometry with thermographic phosphors: Instrumentation and applications," Rev. Sci. Instrum. **68**, 2615–2650 (1997).
[7]D. L. Beshears, D. Sitter, W. H. Andrews, M. L. Simpson, R. Abston, M. Cates, and S. W. Allison, "Phosphor thermometry system," U.S. patent 6,123,455 (26 September 2000).
[8]C. D. S. Brites, A. Millán, and L. D. Carlos, "Lanthanides in luminescent thermometry," in *Handbook on the Physics and Chemistry of Rare Earths*, edited by J.-C. Bunzli, and V. K. Pecharsky (Elsevier, 2016), pp. 339–427.
[9]G. H. Dieke, H. M. Crosswhite, and B. Dunn, "Emission spectra of the doubly and triply ionized rare earths," J. Opt. Soc. Am. **51**, 820 (1961).
[10]C. D. S. Brites, P. P. Lima, N. J. O. Silva, A. Millán, V. S. Amaral, F. Palacio, and L. D. Carlos, "Thermometry at the nanoscale," Nanoscale **4**, 4799 (2012).
[11]A. Ćirić, T. Gavrilović, and M. D. Dramićanin, "Luminescence intensity ratio thermometry with Er^{3+}: Performance overview," Crystals **11**, 189 (2021).
[12]M. Dramićanin, "Introduction to measurements of temperature," in *Luminescent Thermometry* (Elsevier, 2018), pp. 1–12.
[13]T. Zheng, M. Runowski, N. Stopikowska, M. Skwierczyńska, S. Lis, P. Du, and L. Luo, "Dual-center thermochromic Bi_2MoO_6:Yb^{3+}, Er^{3+}, Tm^{3+} phosphors for ultrasensitive luminescence thermometry," J. Alloys Compd. **890**, 161830 (2022).
[14]A. Ćirić, J. Aleksić, T. Barudžija, Ž Antić, V. Đorđević, M. Medić, J. Periša, I. Zeković, M. Mitrić, and M. D. Dramićanin, "Comparison of three ratiometric temperature readings from the Er^{3+} upconversion emission," Nanomaterials **10**, 627–610 (2020).
[15]A. M. Kaczmarek, M. Suta, H. Rijckaert, A. Abalymov, I. Van Driessche, A. G. Skirtach, A. Meijerink, and P. Van Der Voort, "Visible and NIR upconverting Er^{3+}–Yb^{3+} luminescent nanorattles and other hybrid PMO-inorganic structures for *in vivo* nanothermometry," Adv. Funct. Mater. **30**, 2003101 (2020).
[16]J. Periša, Z. Ristić, W. Piotrowski, Ž Antić, L. Marciniak, and M. D. Dramićanin, "All near-infrared multiparametric luminescence thermometry using Er^{3+}, Yb^{3+}-doped YAG nanoparticles," RSC Adv. **11**, 15933–15942 (2021).
[17]C. Hazra, A. Skripka, S. J. L. Ribeiro, and F. Vetrone, "Erbium single-band nanothermometry in the third biological imaging window: Potential and limitations," Adv. Opt. Mater. **8**, 2001178 (2020).
[18]J. R. Lakowicz, *Principles of Fluorescence Spectroscopy* (Springer, 2006).
[19]B. del Rosal, E. Ximendes, U. Rocha, and D. Jaque, "*In vivo* luminescence nanothermometry: From materials to applications," Adv. Opt. Mater. **5**, 1600508 (2017).
[20]A. Ćirić, J. Periša, I. Zeković, Ž Antić, and M. D. Dramićanin, "Multilevel-cascade intensity ratio temperature read-out of Dy^{3+} luminescence thermometers," J. Lumin. **245**, 118795 (2022).
[21]X. Tian, X. Wei, Y. Chen, C. Duan, and M. Yin, "Temperature sensor based on ladder-level assisted thermal coupling and thermal-enhanced luminescence in $NaYF_4$:Nd^{3+}," Opt. Express **22**, 30333 (2014).
[22]L. Li, F. Qin, Y. Zhou, Y. Zheng, J. Miao, and Z. Zhang, "Three-energy-level-cascaded strategy for a more sensitive luminescence ratiometric thermometry," Sens. Actuators, A **304**, 111864 (2020).
[23]D. Yu, H. Li, D. Zhang, Q. Zhang, A. Meijerink, and M. Suta, "One ion to catch them all: Targeted high-precision Boltzmann thermometry over a wide temperature range with Gd^{3+}," Light: Sci. Appl. **10**, 236 (2021).
[24]P. Netzsch, M. Hämmer, E. Turgunbajew, T. P. van Swieten, A. Meijerink, H. A. Höppe, and M. Suta, "Beyond the energy gap law: The influence of selection rules and host compound effects on nonradiative transition rates in Boltzmann thermometers," Adv. Opt. Mater. **10**, 2200059 (2022).
[25]M. Suta and A. Meijerink, "A theoretical framework for ratiometric single ion luminescent thermometers—Thermodynamic and kinetic guidelines for optimized performance," Adv. Theory Simul. **3**, 2000176 (2020).
[26]R. G. Geitenbeek, H. W. de Wijn, and A. Meijerink, "Non-Boltzmann luminescence in Na_yF_4:Eu^{3+}: Implications for luminescence thermometry," Phys. Rev. Appl. **10**, 1 (2018).
[27]A. S. Souza, L. A. O. Nunes, I. G. N. Silva, F. A. M. Oliveira, L. L. da Luz, H. F. Brito, M. C. F. C. Felinto, R. A. S. Ferreira, S. A. Júnior, L. D. Carlos, and O. L. Malta, "Highly-sensitive Eu^{3+} ratiometric thermometers based on excited state absorption with predictable calibration," Nanoscale **8**, 5327–5333 (2016).
[28]A. Ćirić, I. Zeković, M. Medić, Ž Antić, and M. D. Dramićanin, "Juddofelt modelling of the dual-excited single band ratiometric luminescence thermometry," J. Lumin. **225**, 117369 (2020).
[29]J. Drabik and L. Marciniak, "KLa_4O_{12}:Tb^{3+} nanocrystals for luminescent thermometry in a single-band-ratiometric approach," ACS Appl. Nano Mater. **3**, 3798–3806 (2020).
[30]J. Stefanska and L. Marciniak, "Single-band ratiometric luminescent thermometry using Pr^{3+} ions emitting in yellow and red spectral ranges," Adv. Photonics Res. **2**, 2100070 (2021).
[31]M. D. Dramićanin, "Trends in luminescence thermometry," J. Appl. Phys. **128**, 040902 (2020).
[32]A. Ćirić, Ł Marciniak, and M. D. Dramićanin, "Luminescence intensity ratio squared—A new luminescence thermometry method for enhanced sensitivity," J. Appl. Phys. **131**, 114501 (2022).
[33]G. Kortüm, W. Braun, and G. Herzog, "Principles and techniques of diffuse-reflectance spectroscopy," Angew. Chem. Int. Ed. Engl. **2**, 333–341 (1963).
[34]Q. Wang, M. Liao, Q. Lin, M. Xiong, Z. Mu, and F. Wu, "A review on fluorescence intensity ratio thermometer based on rare-earth and transition metal ions doped inorganic luminescent materials," J. Alloys Compd. **850**, 156744 (2021).
[35]C. D. S. Brites, S. Balabhadra, and L. D. Carlos, "Lanthanide-based thermometers: At the cutting-edge of luminescence thermometry," Adv. Opt. Mater. **7**, 1801239 (2019).
[36]G. Fantner, see https://www.epfl.ch/labs/lben/wp-content/uploads/2018/07/Error-Propagation_2013.pdf for "A brief introduction to error analysis and propagation" (2011) (last accessed March 13, 2022).
[37]T. P. van Swieten, A. Meijerink, and F. T. Rabouw, "Impact of noise and background on measurement uncertainties in luminescence thermometry," ACS Photonics **9** , 1366 (2022).
[38]A. A. Kalinichev, M. A. Kurochkin, A. Y. Kolomytsev, R. S. Khasbieva, E. Y. Kolesnikov, E. Lähderanta, and I. E. Kolesnikov, "Yb^{3+}/Er^{3+}-codoped GeO_2–PbO–PbF_2 glass ceramics for ratiometric upconversion temperature sensing based on thermally and non-thermally coupled levels," Opt. Mater. **90**, 200–207 (2019).
[39]F. Auzel, "Compteur quantique par transfert d'energie entre deux ions de terres rares dans un tungstate mixte et dans un verre," C. R. Acad. Sci. Paris **262**, 1016–1019 (1966).
[40]F. Auzel, "Upconversion and anti-Stokes processes with f and d ions in solids," Chem. Rev. **104**, 139–174 (2004).
[41]W. T. Carnall, H. Crosswhite, and H. M. Crosswhite, "Energy level structure and transition probabilities in the spectra of the trivalent lanthanides in LaF_3" (Argonne National Laboratory, IL, 1978).
[42]V. V. Ter-Mikirtychev and V. A. Fromzel, "Directly single-diode-pumped continuous-wave Yb^{3+}:YAG laser tunable in the 1047–1051-nm wavelength range," Appl. Opt. **39**, 4964 (2000).
[43]A. A. Kaminskii, *Crystalline Lasers Physical Processes and Operating Schemes* (CRC Press, 2020).
[44]M. Zeng, F. Artizzu, J. Liu, S. Singh, F. Locardi, D. Mara, Z. Hens, and R. Van Deun, "Boosting the Er^{3+} 1.5 μm luminescence in $CsPbCl_3$ perovskite nanocrystals for photonic devices operating at telecommunication wavelengths," ACS Appl. Nano Mater. **3**, 4699–4707 (2020).
[45]A. Yoshikawa, G. Boulon, L. Laversenne, H. Canibano, K. Lebbou, A. Collombet, Y. Guyot, and T. Fukuda, "Growth and spectroscopic analysis

of Yb^{3+}-doped $Y_3Al_5O_{12}$ fiber single crystals," J. Appl. Phys. **94**, 5479–5488 (2003).
[46]A. Ćirić and M. D. Dramićanin, "LumTHools—software for fitting the temperature dependence of luminescence emission intensity, lifetime, bandshift, and bandwidth and luminescence thermometry and review of the theoretical models," J. Lumin. **252**, 119413 (2022).
[47]S. H. Chung, A. E. Cerussi, S. I. Merritt, J. Ruth, and B. J. Tromberg, "Non-invasive tissue temperature measurements based on quantitative diffuse optical spectroscopy (DOS) of water," Phys. Med. Biol. **55**, 3753–3765 (2010).
[48]A. Bednarkiewicz, L. Marciniak, L. D. Carlos, and D. Jaque, "Standardizing luminescence nanothermometry for biomedical applications," Nanoscale **12**, 14405–14421 (2020).